Spectroscopy of Four Cataclysmic Variables with Periods above 7 Hours [1]

Christopher S. Peters and John R. Thorstensen

Department of Physics and Astronomy
6127 Wilder Laboratory, Dartmouth College
Hanover, NH 03755-3528;
christopher.s.peters@dartmouth.edu
john.thorstensen@dartmouth.edu

ABSTRACT

We present spectroscopy of four cataclysmic variables. Using radial velocity measurements, we find orbital periods P_{orb} for the first time. The stars and their periods are GY Hya, 0.347230(9) d; SDSS J204448-045929, 1.68(1) d; V392 Hya, 0.324952(5) d; and RX J1951.7+3716, 0.492(1) d. We also detect the spectra of the secondary stars, estimate their spectral types, and derive distances based on surface brightness and Roche lobe constraints.

Subject headings: Stars: Binaries: Spectroscopic, Stars: dwarf novae, Cataclysmic Variables

1. Introduction

Cataclysmic variables (CVs) are close binary star systems comprised of a white dwarf (the primary) that accretes matter from a less compact companion star (the secondary) in Roche lobe overflow. There exist many types of CVs, providing unique laboratories in which to study various aspects of astrophysics. Warner (1995) gives an overview of the field.

The most fundamental characteristic of a CV is the period of its orbit, P_{orb}. When an eclipse is evident, the period is incontrovertible. In non-eclipsing CVs, the period may be found using radial velocities. Often, a spectral contribution from the secondary star is present. This provides useful clues to the distance and the evolutionary state of the system.

In the current study, we discuss four CVs: GY Hya, SDSS J204448-045929, V392 Hya, and RXJ1951.7+3716. None of them have extensive spectroscopic studies in the literature. We report their basic properties (period, spectral type of secondary) and infer distances. All four stars have

---

[1]Based on observations obtained at the MDM Observatory, operated by Dartmouth College, Columbia University, Ohio State University, and the University of Michigan.

periods above 7 hours, the longest period being that of SDSS J204448-045929, $P_{\mathrm{orb}} = 1.68(1)$ d. As stated in Thorstensen, Fenton, & Taylor (2004) (hereafter TFT04), longer-period systems provide information on CV evolution; in particular, many systems appear to have begun nuclear evolution prior to mass transfer (Baraffe & Kolb 2000). TFT04 provide a background in long-period CV analysis.

Section 2 describes the observations and analysis, and §3 gives results. In §4, we provide a brief discussion.

2. Techniques

Table 1 lists the observations, all of which were taken with the 2.4-meter Hiltner telescope at MDM Observatory in Kitt Peak, Arizona. We used the 'modular' spectrograph, a 600 line mm^{-1} grating, a 1-arcsec slit, and a SITe 2048^2 CCD detector yielding 2 Å pixel^{-1} from 4210 to 7560 Å (vignetting severely toward the ends), and typical resolution of 3.5 Å FWHM. On most observing runs, spectra of comparison lamps were taken whenever the telescope was moved to achieve accurate wavelength calibration. On some observing runs, comparison lamp spectra were not taken during the night, and the wavelength solution derived from lamps was shifted by an amount determined from the night-sky lines. For a detailed discussion of calibration procedures, see TFT04.

2.1. Period Determination

Our main objective was to find orbital periods. To this end, we measured radial velocities in the spectra using both absorption and emission lines, when possible. The absorption lines originate in the atmosphere of the secondary star. Absorption line velocities were found using the IRAF cross-correlation radial velocity package *xcsao* (Kurtz & Mink 1998). The routine was run on the wavelength range 6000 to 6500 Å. Uncertainties, based on the R-statistic of Tonry & Davis (1979), are typically less than 10 km s^{-1}. For a handful of low signal-to-noise exposures, the cross-correlations were not formally significant, leading to unphysical velocities which were excluded from further analyses.

Emission line velocities were found by measuring the shift of Hα via the convolution technique of Schneider & Young (1980) and Shafter (1983). This method consists of convolving two antisymmetric Gaussians with the emission line, with an adjustable separation parameter, α, and searching for the zero of the convolution. Typical values of α are 12-15 Å. The idea (valid or not) is that the two Gaussians measure the wings of the line, which may arise in a symmetrical portion of the accretion-disk emission close to the white dwarf. The best parameters for the convolution function are found by searching for the largest value of α which yields reliable results. This was done for all stars, regardless of line profile (single- or double-peaked).

We ran a period-search algorithm which fit general least-squares sinusoids of the form

$$v(t) = A\cos(\omega t) + B\sin(\omega t) + C$$

to the time series with a range of equally-spaced frequencies, ω. Ideally, a periodogram of $1/\chi^2$ versus frequency shows a lone peak corresponding to the true frequency. Due to the uneven sampling of the time-series, alias (false) periods often appear in the periodogram. We used a Monte Carlo algorithm developed by Thorstensen & Freed (1985) to assess confidence with which the highest peak in the periodogram can be identified with the true orbital frequency. Once the optimal period was found, we fit the time-series with sinusoids of the form

$$v(t) = \gamma + K\sin[2\pi(t - T_0)/P]$$

using a hybrid linear least-square algorithm. This procedure is described in detail in TFT04.

In Figure 1, radial velocity curves are shown, folded twice for continuity. When both absorption and emission line velocities are available, the radial velocity curves are folded using the weighted mean period. The parameters for the least-squares best-fit curves are given in Table 4. The absorption and emission line curves are very close to being $\frac{1}{2}$ cycle out-of-phase. If the curves are consistent with $\Delta\phi = 0.5$, the mass ratio of the secondary to the primary may be estimated to be $q = M_2/M_1 = K_1/K_2$. We caution the reader that the measured K values may misrepresent the orbital motion of the components, especially K_1 which originates from the accretion disk. Having the emission and absorption velocities $\frac{1}{2}$ cycle out-of-phase is a necessary, but not sufficient condition for the K_1 to represent the motion of the white dwarf.

2.2. Spectral Decomposition

For spectral decomposition, we prepared an average spectrum for each system in which the individual exposures were shifted to the absorption line rest frame. We have a collection of standard K- and M-star obtained with the same instrumental setup as the present data. These K and M stars were classified by Keenan & McNeil (1989) and Boeshaar (1976), respectively. The library of template spectra were scaled and subsequently subtracted from the averaged spectra in order to eliminate the absorption lines due to the secondary. We did not rotationally-broaden our template spectra prior to subtraction because the rotational broadening expected for the secondary stars is small compared to our spectral resolution. We examined the residual spectra by eye. In an ideal case, the absorption lines would disappear entirely, leaving only the continuum and emission lines, but in reality the subtractions were never perfect. Nonetheless, the subtractions were fairly good. In all the cases considered here, the spectral type of the secondary could be estimated to ± 1 subclass, and the secondary's contribution to the flux could be estimated to $\pm 15\%$.

Using the known periods and spectral types, inferences about the systems have been made based on physical considerations and empirical relations. We assumed that the secondaries fill their

Roche lobes, and are undergoing mass transfer. Note carefully that we *did not* assume that the secondaries follow a main-sequence spectral type versus absolute magnitude (sp-M_V) relationship. Instead, we used a relationship between the surface brightness and the spectral type for normal stars derived by Beuermann (private communication 2004). To convert the surface brightness to M_V, we of course need a secondary-star radius R_2. This is strongly constrained by the Roche geometry and the orbital period. To estimate R_2 we begin with an analytical approximation to the Roche lobe radius, given by Beuermann et al. (1998), which shows that, at a given P_{orb}, R_2 is almost independent of the primary star mass M_1, and is dependent only on the cube root of M_2. We have no direct measure of M_2, but we can estimate a range of plausible values using the evolutionary scenarios of Baraffe & Kolb (2000) as a guideline, at least for systems with $P_{orb} < 10$ h. Armed with our estimate of the secondary's radius, we transformed the surface brightness to M_V. The synthetic apparent magnitude of the secondary, m_V, was found from the scaled template spectra used during spectral decomposition using the IRAF task *sbands* and the Bessell (1990) tabulation of the V passband. Finally, visual extinction values, A_V, were estimated from infrared dust maps of Schlegel, Finkbeiner, & Davis (1998), and A_V, m_V, and M_V were combined to yield a distance. The dust extinction estimate is imperfect, because (a) the ISM can be patchy on scales smaller than the 6-arcmin resolution of the maps, and (b) the maps give estimates of the total extinction to the edge of the Galaxy, rather than to the star of interest. However, for three of the four objects studied here, the Galactic latitudes are high enough that the uncertain extinction should have a fairly minor effect on the distance.

3. The Individual Stars

Our results are summarized in tables and figures. Table 2 shows measurements of spectral line properties based on flux-averaged spectra. All radial velocity measurements included in the analysis are listed in Table 3. Table 4 lists parameters of the best-fit sinusoids to the velocity time series. Table 5 shows derived characteristics of the secondary and inferred distances. Fig. 1 shows folded radial velocity curves, Fig. 2 displays the spectrum of V392 Hya during two separate observing runs, and Fig. 3 shows the flux-averaged spectra of the four objects before and after spectral decomposition.

3.1. GY Hya

Downes et al. (2001) list GY Hya as an unconfirmed U Gem star, a subclass of dwarf nova (DN). Zwitter & Munari (1996) obtained a spectrum; strong emission from Hα, Hβ, and HeII were present. Our spectroscopic observations span a baseline of 111 days. Our spectrum (Fig. 3) shows weaker emission features and strong absorption lines, indicating a significant contribution from the secondary. The absorption line velocities have large amplitude ($K_2 \sim 180$ km s^{-1}) and small scatter about a best-fit sinusoid of period, $P_{orb} = 0.347230(9)$ d, or 500 min. A Monte Carlo

simulation yields a discriminatory power of 98% for this P_{orb}. Time-series photometry from Monard (private communication 2005) shows an eclipse with a period of $P_{orb} = 0.347237(1)$ d; our period is consistent with this. The emission lines were weak, thus a reliable fit to the Hα emission line velocities was not found and not included in Fig. 1.

Spectral decomposition of our flux-averaged spectrum shows a secondary of type K4 or K5. The synthetic V magnitude of the secondary based on the decomposition is 16.7 ± 0.2. This uncertainty includes both the uncertainty in spectral type and also in the factors used to multiply the template spectra. The P_{orb} falls within the range of evolutionary scenarios considered by Baraffe & Kolb (2000), so for purposes of defining the Roche lobe, we estimate $M_2 = 0.65 \pm 0.10$ M$_\odot$. This corresponds to $R_2 = 0.84 \pm 0.05$ R$_\odot$ at this P_{orb}, which using surface brightnesses from Beuermann (private communication 2004) in turn implies $M_V = 5.9 \pm 0.2$. Assuming an extinction $A_V = 0.3$, this yielded a distance of 1260^{+190}_{-160} pc.

With no reliable emission line velocities, an estimate of the mass ratio could not be made. The fact that GY Hya is an eclipsing system constrains the inclination to be greater than ~ 70 degrees. The available evidence does not suggest that the masses are unusual; for example, with $q \leq 1$ and $M_2 = 0.65 \pm 0.10$ M$_\odot$, there is a comfortable fit with $i = 80$ degrees at $M_1 = 0.7$ M$_\odot$ and $M_2 = 0.65$ M$_\odot$.

3.2.   SDSS J204448-045929

The subclass of SDSS J204448-045929 (SDSS 2044, for brevity) is unknown, as it was recently discovered as a CV in the Sloan Digital Sky Survey (Szkody et al. 2003). Our data span 10 days and had high signal-to-noise (S/N) ratios. The spectra showed intrinsically strong and narrow emission lines, most notably Hα. Both the absorption and emission line velocities are measureable, although amplitudes are low. The orbital period, $P_{orb} = 1.68(1)$ d, is unusually long for a CV. According to the *The Catalog and Atlas of CVs: The Living Edition* (Downes et al. 2001), only 7% of CVs with known periods (440 total, including SDSS 2044) have periods above 9 hours. However, a 97% Monte Carlo discriminatory power shows that our preferred period is very likely to be correct.

We find that the absorption and emission line radial velocity curves in Figure 1 are consistent with $\Delta\phi = 0.5$. This allows us to estimate a mass ratio, $q = 0.36^{+0.13}_{-0.12}$. Given that the mass of the white dwarf needs to be less than the Chandrasekhar limit of 1.4 M$_\odot$, this requires that the secondary have a mass ≤ 0.7 M$_\odot$. The period of SDSS 2044 (~ 40 h) is well above the 10.0 h upper limit of the evolutionary scenarios of Baraffe & Kolb (2000), so we could not use their results. Given the above mass ratio constraints, we adopt a conservative range of mass for the secondary to be $M_2 = 0.4 \pm 0.3$ M$_\odot$. The secondary's radius is dependent upon the cube-root of the mass, so the although the uncertainty in mass is large, the radius uncertainty is not: $R_2 = 1.9 \pm 0.5$ R$_\odot$ at $P_{orb} = 1.68(1)$ d. Given the range in q and a conservative range in white dwarf mass of $M_1 = 0.9 \pm 0.4$ M$_\odot$, the inclination is within 45 ± 10 degrees.

A clean spectral decomposition gives a secondary spectral type of K4 or K5, with corresponding synthetic V apparent magnitude of 18.4 ± 0.2. Using the radius for the secondary, the surface brightness is transformed into an absolute magnitude of $M_V = 7.5 \pm 0.7$. With an extinction of $A_V = 0.2$, we find a distance of 1380^{+530}_{-380} pc.

3.3. V392 Hya

Similar to GY Hya, V392 Hya is also listed by Downes et al. (2001) as an unconfirmed U Gem star (DN). V392 Hya, or EC 10565-2858, was discovered in the Edinburgh-Cape Blue Object Survey. Chen et al. (2001) show a spectrum that spans $\lambda\lambda$ 3800-5000 Å; our spectral range is 4210-7560Å. Therefore, comparison is limited; the only spectral feature in common is Hβ emission. Chen et al. (2001) report two periods, ~ 8 h and ~ 12 h, derived from time-resolved spectroscopy. Due to gaps in their time series, they were unable to distinguish between the two periods. Our time series is comprised of a lone observation in 2002, followed a year later by 4 consecutive nights, and finally 6 nights scattered through 2004.

Figure 2 shows V392 Hya in two different states during January 2004 and February 2003. This is evident from the continua. The mean flux level differs by a factor of ~ 4. Differences in spectral features are seen, most notably the strength of Hα emission and the structure of the Hβ line. As shown in Table 2 and Figure 2, the Hα line becomes thinner and stronger by a factor of ~ 2 in outburst. The Hβ line changes from emission superposed on flat continuum during the lower state to emission superposed on a wider absorption line during the higher state. This is commonly thought to be due to the optically thick accretion disk.

Despite the different states, the absorption line velocities from the late-type secondary are measureable in all our data and yield a best-fit period of $P_{\text{orb}} = 0.324952(5)$ d, or 468 min. A Monte Carlo simulation to discriminate between alias periods returns a confidence level of $\sim 90\%$, which is the lowest for the stars presented in this paper. Emission line velocities based on Hα had more scatter about the best-fit curve than the absorption line velocities, but fit reasonably well, as seen in Figure 1. The radial velocity curves for V392 Hya are also consistent with $\Delta\phi = 0.5$, leading to an estimate of $q = 0.55 \pm 0.15$. This constrains the inclination to be $i = 45 \pm 13$ degrees, assuming a conservative white dwarf mass of $M_1 = 0.9 \pm 0.4$ M$_\odot$.

Spectral decomposition was done using the observations in quiescence since the absorption lines (due to the secondary star) were more prominent. Visual inspection led to an inferred secondary of spectral type K5 or K6, with corresponding synthetic V magnitude of $m_V = 18.9 \pm 0.2$. A K5/6 secondary with a period of ~ 7.8 h implied (using Baraffe & Kolb (2000)) a mass and radius of 0.60 ± 0.05 M$_\odot$ and 0.78 ± 0.03 R$_\odot$, respectively. This radius translated the surface brightness calculation of Beuermann (private communication 2004) into an absolute magnitude of $M_V = 6.0 \pm 0.2$, which, when combined with an extinction of 0.2 magnitudes and m_V, gave an inferred distance of 3470^{+510}_{-450} pc.

3.4. RXJ1951.7+3716

Motch et al. (1998) classify RXJ1951.7+3716 (RX 1951, hereafter) as a CV, with no specified subclass. Our data span 10 days in 2001, with coverage over an 8-hour range in hour angle to discriminate the daily cycle alias. The mean flux level for the spectra is ≥ 2.5 times higher than the other three objects in this paper. In Figure 3, the small difference between the upper and lower spectra shows the weak, but present, contribution from the secondary.

The emission lines (particularly Hα and Hβ) are strong and narrow, yielding small uncertainty in emission line velocities (see Table 3). Despite the weakness of the secondary contribution, absorption line velocities are measurable. The weighted mean period found is $P_{\mathrm{orb}} = 0.492(1)$ d. Monte Carlo simulations rule out other alias periods with a discriminatory power of $\geq 90\%$. With a small K_2 of 81 ± 7 km s^{-1}, the inclination is expected to be low. We find that for a white dwarf mass range of 0.9 ± 0.4 M$_\odot$ and $q \leq 1$, $i = 25 \pm 10$ degrees.

The spectral type of the secondary is estimated to be K7.5 or M0.5; the lower spectrum in Figure 3 is after an M0.5 star has been subtracted. The synthetic magnitude calculated for the secondary star is $m_V = 17.6 \pm 0.2$. A secondary mass of 0.6 ± 0.3 M$_\odot$ is extrapolated from Baraffe & Kolb (2000) since the period lies slightly above the cutoff of 10.0 hours. At $P_{\mathrm{orb}} = 0.492(1)$ d, this mass range corresponds to a radius of $R_2 = 0.99 \pm 0.18$ R$_\odot$. Beuermann (private communication 2004) surface brightnesses were converted into an absolute magnitude of $M_V = 7.4 \pm 0.6$. The extinction value used is large ($A_V = 0.8$) due to the fact that RX 1951 is only ~ 5 degrees from the Galactic plane. We find RX 1951 to be at a distance of 760^{+240}_{-180} pc. It is not surprising to find that this source is closer than the other three due to its greater apparent brightness.

4. Discussion

We find orbital periods for these four systems to be above 7 hours; the period of SDSS 2044, $P_{\mathrm{orb}} = 1.68(1)$ d is notably long for a CV. In longer-period systems, the secondaries are usually cooler than expected for main-sequence stars filling their Roche lobes at the observed period (Beuermann et al. 1998). Referring to the plot of spectral type vs. period in Baraffe & Kolb (2000), it is clear that the four secondary stars in this paper do not lie on zero-age main sequence (ZAMS) evolutionary tracks, but rather are significantly cooler, most likely due to commencement of nuclear evolution prior to the onset of mass transfer (Baraffe & Kolb 2000). Although the models of Baraffe & Kolb (2000) do not apply to periods above 10 hours, and thus may not be directly applied to SDSS 2044 and RX 1951, these two systems are the furthest from the ZAMS.

The systems in this paper have been selected based on their longer periods. Therefore, they do not represent the full range in CV periods. For example, dwarf novae with hydrogen-rich secondaries have periods as short as 75 minutes. A goal of studying CVs is to obtain an accurate catalog of their population. To do so, different methods of CV discovery are essential, as is evident from

the subset presently studied. V392 Hya was identified in the Edinburgh-Cape Blue Object Survey, while SDSS 2044 and RX 1951 were discovered by SDSS and ROSAT, respectively. The wide range in techniques and energies is beneficial for finding these systems.

We find distances to the CVs via spectroscopic parallax. This method relies on surface brightness calculations of the secondary star filling its Roche lobe, but more importantly upon accurate identification of the secondary's spectral type. We are able to detect and deduce the spectral type (via spectral decomposition) of the secondary star to within one subclass. This is sufficient to yield distances with 15% uncertainty in favorable cases.

REFERENCES

Baraffe, I., Kolb, U. 2000, MNRAS, 318, 354

Bessell, M. S. 1990, PASP, 102, 1181

Beuermann, K., Baraffe, I., Kolb, U., and Weichhold, M. 1998, A&A, 339, 518

Beuermann, K. 2004, Private Communication

Boeshaar, P. 1976, Ph. D. thesis, Ohio State University

Chen, A., O'Donoghue, D.O., Stobie, R.S., Kilkenny, D., & Warner, B. 2001, MNRAS, 325, 89

Downes, R., Webbink, R., Shara, M., Ritter, H., Kolb, U., and Duerbeck, H. 2001, PASP, 113, 764

Keenan, P. C., & McNeil, R. C. 1989, ApJS, 71, 245

Kurtz, M. J. & Mink, D. J. 1998, PASP, 110, 934

Monard, B. 2005, Private Communication

Motch, C., et al. 1998, A&AS, 132, 341

Schlegel, D. J., Finkbeiner, D. P., & Davis, M. 1998, ApJ, 500, 525

Schneider, D. and Young, P. 1980, ApJ, 238, 946

Shafter, A. W. 1983, ApJ, 267, 222

Szkody, P., et al. 2003, AJ, 126, 1499

Thorstensen, J. R., Freed, I. W. 1985, AJ, 90, 2082

Thorstensen, J. R., Fenton, W. H. and Taylor, C. J. 2004, PASP, 116, 300

Tonry, J. & Davis, M. 1979, AJ, 84, 1511

Warner, B., in *Cataclysmic Variable Stars*, 1995, Cambridge University Press, New York

Zwitter, T. & Munari, U. 1996, A&AS, 117, 449

Table 1.   Journal of Observations

Date [UT]	N	HA (start) [hh:mm]	HA (end) [hh:mm]
GY Hya:			
2004 Mar 7	8	$-2:05$	$+1:36$
2004 Mar 9	9	$-0:33$	$+1:29$
2004 Jun 22	3	$-0:15$	$+2:21$
2004 Jun 25	2	$+0:02$	$+0:15$
2004 Jun 26	1	$-0:06$	$-0:06$
2004 Jul 1	2	$+0:18$	$+0:35$
SDSS 2044-04:			
2004 Jun 22	2	$-1:58$	$-1:47$
2004 Jun 23	3	$-1:24$	$-1:05$
2004 Jun 24	4	$-0:39$	$+1:14$
2004 Jun 25	3	$-2:13$	$+0:43$
2004 Jun 26	5	$-3:08$	$+0:30$
2004 Jun 27	2	$+0:55$	$+1:07$
2004 Jun 28	6	$-2:19$	$+1:20$
2004 Jun 29	2	$-3:41$	$-3:29$
2004 Jun 30	1	$+1:33$	$+1:33$
2004 Jul 1	2	$-3:02$	$-2:49$
V392 Hya:			
2002 Jan 22	2	$+0:07$	$+0:18$
2003 Jan 31	1	$+0:17$	$+0:17$
2003 Feb 1	3	$-1:21$	$+2:42$
2003 Feb 2	2	$-0:10$	$+1:11$
2003 Feb 3	5	$-2:44$	$-1:07$
2004 Jan 13	1	$-1:23$	$-1:23$

Table 1—Continued

Date [UT]	N	HA (start) [hh:mm]	HA (end) [hh:mm]
2004 Jan 16	1	$-0:58$	$-0:58$
2004 Jan 17	1	$+2:12$	$+2:12$
2004 Jan 18	1	$-0:47$	$-0:47$
2004 Jan 19	1	$+2:47$	$+2:47$
2004 Mar 7	1	$+1:58$	$+1:58$
RX 1951:			
2001 Jun 23	2	$+0:52$	$+0:57$
2001 Jun 24	1	$+2:07$	$+2:07$
2001 Jun 25	3	$-2:02$	$+2:02$
2001 Jun 26	5	$-4:38$	$+2:15$
2001 Jun 27	3	$-2:03$	$+2:19$
2001 Jun 28	4	$-5:19$	$+2:37$
2001 Jun 29	2	$-1:19$	$+2:28$
2001 Jul 1	4	$-4:52$	$+2:44$
2001 Jul 2	2	$+1:06$	$+2:45$

Table 2.   Emission Features

Feature	E.W.[a] (Å)	Flux[b] (10^{-16} erg cm^{-2} s^{1})	FWHM [c] (Å)
		GY Hya:	
Hβ	7	86	22
NaD	-6	-93	13
Hα	9	122	28
		SDSS 2044-04:	
Hγ	28	84	17
HeI $\lambda 4471$	7	22	13
Hβ	17	64	12
HeI $\lambda 5015$	3	9	13
HeI $\lambda 5876$	6	26	14
Hα	21	95	10
HeI $\lambda 6678$	3	13	18
HeI $\lambda 7067$	4	15	19
		V392 Hya (high state):	
Hγ	1	53	6
HeII $\lambda 4686$	1	25	11
Hβ	3	106	12
HeI $\lambda 5876$	1	8	9
NaD	-1	-29	13
Hα	7	155	15
HeI $\lambda 6678$	1	21	17
		V392 Hya (low state):	
Hβ	12	80	20

Table 2—Continued

Feature	E.W.[a] (Å)	Flux[b] (10^{-16} erg cm^{-2} s^1)	FWHM [c] (Å)
HeI λ5876	1	7	11
NaD	−2	−11	12
Hα	14	77	19
HeI λ6678	2	8	28

RX 1951:

Hγ	21	945	13
HeI λ4471	9	378	18
HeII λ4686	3	113	17
Hβ	26	1010	13
HeI λ4921	4	169	15
HeI λ5015	3	131	12
Fe λ5169	3	115	13
HeI λ5876	7	237	12
NaD	−1	−38	12
Hα	29	922	13
HeI λ6678	4	110	15
HeI λ7067	4	108	17

[a]Emission equivalent widths are counted as positive.

[b]Absolute line fluxes are uncertain by a factor of about 2, but relative fluxes of strong lines are estimated accurate to $\sim$ 10 per cent.

[c]From Gaussian fits.

Table 3.   Radial Velocities

Modified JD	v_{abs}	$\sigma_{v_{\mathrm{abs}}}$	v_{emn}	$\sigma_{v_{\mathrm{emn}}}$
	GY Hya			
53071.8712	51	10	$\cdots$	$\cdots$
53071.8802	70	10	$\cdots$	$\cdots$
53071.9361	175	9	$\cdots$	$\cdots$
53071.9450	171	9	$\cdots$	$\cdots$
53071.9539	175	10	$\cdots$	$\cdots$
53071.9628	160	9	$\cdots$	$\cdots$
53072.0064	120	10	$\cdots$	$\cdots$
53072.0243	42	10	$\cdots$	$\cdots$
53073.9296	-24	8	$\cdots$	$\cdots$
53073.9408	11	6	$\cdots$	$\cdots$
53073.9559	48	11	$\cdots$	$\cdots$
53073.9644	65	8	$\cdots$	$\cdots$
53073.9734	109	7	$\cdots$	$\cdots$
53073.9823	115	9	$\cdots$	$\cdots$
53073.9965	133	9	$\cdots$	$\cdots$
53074.0054	166	9	$\cdots$	$\cdots$
53074.0143	147	10	$\cdots$	$\cdots$
53178.6563	-87	5	$\cdots$	$\cdots$
53178.6653	-115	7	$\cdots$	$\cdots$
53178.7645	-118	6	$\cdots$	$\cdots$
53181.6594	177	9	$\cdots$	$\cdots$
53181.6683	171	9	$\cdots$	$\cdots$
53182.6514	79	7	$\cdots$	$\cdots$
53187.6536	48	7	$\cdots$	$\cdots$
53187.6655	-16	9	$\cdots$	$\cdots$
	SDSS2044:			
53178.8446	15	8	-13	4

Table 3—Continued

Modified JD	v_{abs}	$\sigma_{v_{\mathrm{abs}}}$	v_{emn}	$\sigma_{v_{\mathrm{emn}}}$
53178.8521	15	7	−19	4
53179.8652	−87	7	−11	4
53179.8728	−92	11	−14	4
53179.8786	−116	13	$\cdots$	$\cdots$
53180.8940	62	10	−70	5
53180.9015	49	10	$\cdots$	$\cdots$
53180.9645	84	10	−50	5
53180.9720	96	8	−54	5
53181.8260	−99	7	38	5
53181.8934	−50	7	41	5
53181.9477	−58	5	32	5
53182.7852	79	11	−25	6
53182.7928	57	14	−32	6
53182.8258	55	11	−36	6
53182.8330	28	13	−47	7
53182.9364	−4	9	−10	5
53183.9507	13	6	−37	5
53183.9596	26	9	−48	5
53184.8143	−54	10	−22	5
53184.8232	−57	10	−9	6
53184.9419	−82	9	12	6
53184.9495	−104	11	−5	6
53184.9569	−108	12	$\cdots$	$\cdots$
53184.9656	−87	12	$\cdots$	$\cdots$
53185.7547	52	10	−51	6
53185.7628	42	16	−45	6
53186.9690	−77	5	4	5
53187.7761	85	8	−22	5
53187.7850	67	8	−24	5

V392 Hya

Table 3—Continued

Modified JD	v_{abs}	$\sigma_{v_{\mathrm{abs}}}$	v_{emn}	$\sigma_{v_{\mathrm{emn}}}$
52296.9372	−108	16	78	18
52296.9448	−113	14	44	11
52670.9208	−179	18	130	20
52671.8506	−107	14	15	10
52671.9360	−133	13	18	10
52672.0186	101	12	−65	11
52672.8971	−138	13	38	13
52672.9531	−35	20	⋯	⋯
52673.0392	⋯	⋯	−136	22
52673.7875	−75	29	⋯	⋯
52673.8185	−122	24	⋯	⋯
52673.8330	−86	18	75	22
52673.8473	−163	14	57	24
52673.8548	−154	20	29	21
53017.8900	⋯	⋯	−3	15
53017.8999	5	20	9	15
53020.9094	−116	13	106	13
53022.0388	132	18	−102	16
53022.9115	−60	20	4	14
53024.0574	23	31	3	7
53070.9123	⋯	⋯	40	14
53071.8322	⋯	⋯	5	14
53071.8947	−127	20	27	12
53073.7569	⋯	⋯	−64	10
53073.7679	⋯	⋯	−60	9

RX 1951				
52083.9214	8	14	−41	6
52083.9255	42	16	−50	5
52084.9711	65	12	−49	4
52085.7961	−39	18	⋯	⋯

Table 3—Continued

Modified JD	v_{abs}	$\sigma_{v_{\mathrm{abs}}}$	v_{emn}	$\sigma_{v_{\mathrm{emn}}}$
52085.9276	49	10	−41	4
52085.9650	52	14	−67	7
52086.6848	−102	8	19	4
52086.7143	−129	14	29	4
52086.8356	−12	13	−34	6
52086.9013	35	14	−63	5
52086.9710	38	11	−93	3
52087.7898	−54	9	6	4
52087.8954	70	12	−60	5
52087.9710	35	10	−55	4
52088.6510	−109	19	29	9
52088.7348	−85	11	29	4
52088.9537	55	14	−85	4
52088.9807	53	9	−43	4
52089.8151	15	7	−49	3
52089.9722	28	12	−87	4
52091.6617	−88	9	25	7
52091.8416	57	12	−73	6
52091.9143	24	8	−95	3
52091.9780	−9	12	−38	4
52092.9073	57	10	−87	5
52092.9760	14	12	−36	7

Table 4.   Fits to Radial Velocities

Data set	T_0[a]	P (d)	K[b] (km s^{-1})	γ (km s^{-1})	N	σ[c] (km s^{-1})
GY Hya (abs)	53073.942(2)	0.347230(9)	176(8)	2(5)	25	15
SDSS 2044 (abs)	53182.15(2)	1.68(1)	90(8)	−9(5)	30	16
SDSS 2044 (emn)	53183.03(7)	$\cdots$	32(8)	−16(6)	26	17
V392 Hya (abs)	52673.932(5)	0.324952(5)	144(9)	−3(8)	19	23
V392 Hya (emn)	52673.764(7)	$\cdots$	80(14)	−17(9)	22	26
RX 1951 (abs)	52088.797(8)	0.492(1)	81(7)	−22(5)	26	15
RX 1951 (emn)	52088.57(1)	$\cdots$	54(7)	−25(6)	25	16

Note. — Parameters of least-squares sinusoid fits to the radial velocities, of the form $v(t) = \gamma + K \sin(2\pi(t - T_0)/P)$. Where both emission and absorption velocities are available, the period quoted is the weighted average of the periods derived from separated fits to the two data sets, and the period is only given on the first line.

[a]Heliocentric Julian Date minus 2452000. The epoch is chosen to be near the center of the time interval covered by the data, and within one cycle of an actual observation.

[b]In the text, the absorption and emission line radial velocities are denoted K_2 and K_1, respectively.

[c]Root-mean-square residual of the fit.

Table 5.   Inferences from Secondary Stars

Star	Type	Synthetic m_V (mag)	Assumed M_2[a] $M_\odot$	Deduced R_2 $R_\odot$	M_V[b] (mag)	A_V (mag)	Distance (pc)
GY Hya	K4 or K5	16.7 ± 0.2	0.65 ± 0.10	0.84 ± 0.05	5.9 ± 0.2	0.3	1260^{+190}_{-160}
SDSS 2044	K4 or K5	18.4 ± 0.2	0.4 ± 0.3[c]	1.9 ± 0.5	7.5 ± 0.7	0.2	1380^{+530}_{-380}
V392 Hya	K5 or K6	18.9 ± 0.2	0.60 ± 0.05	0.78 ± 0.03	6.0 ± 0.2	0.2	3470^{+510}_{-450}
RX 1951	K7.5 or M0.5	17.6 ± 0.2	0.6 ± 0.3[c]	0.99 ± 0.18	7.4 ± 0.6	0.8	760^{+240}_{-180}

[a]Note carefully that these masses are not measured, but are estimates guided by the models of Baraffe & Kolb (2000). They are used *only* to constrain R_2, which depends only on the cube root of M_2, so this does not contribute substantially to the error budget.

[b]Absolute visual magnitude inferred for the secondary alone, on the basis of surface brightness and Roche lobe size (see text.)

[c]The period is above the limit of evolutionary scenarios computed by Baraffe & Kolb (2000), so a conservative estimate of the mass is made.
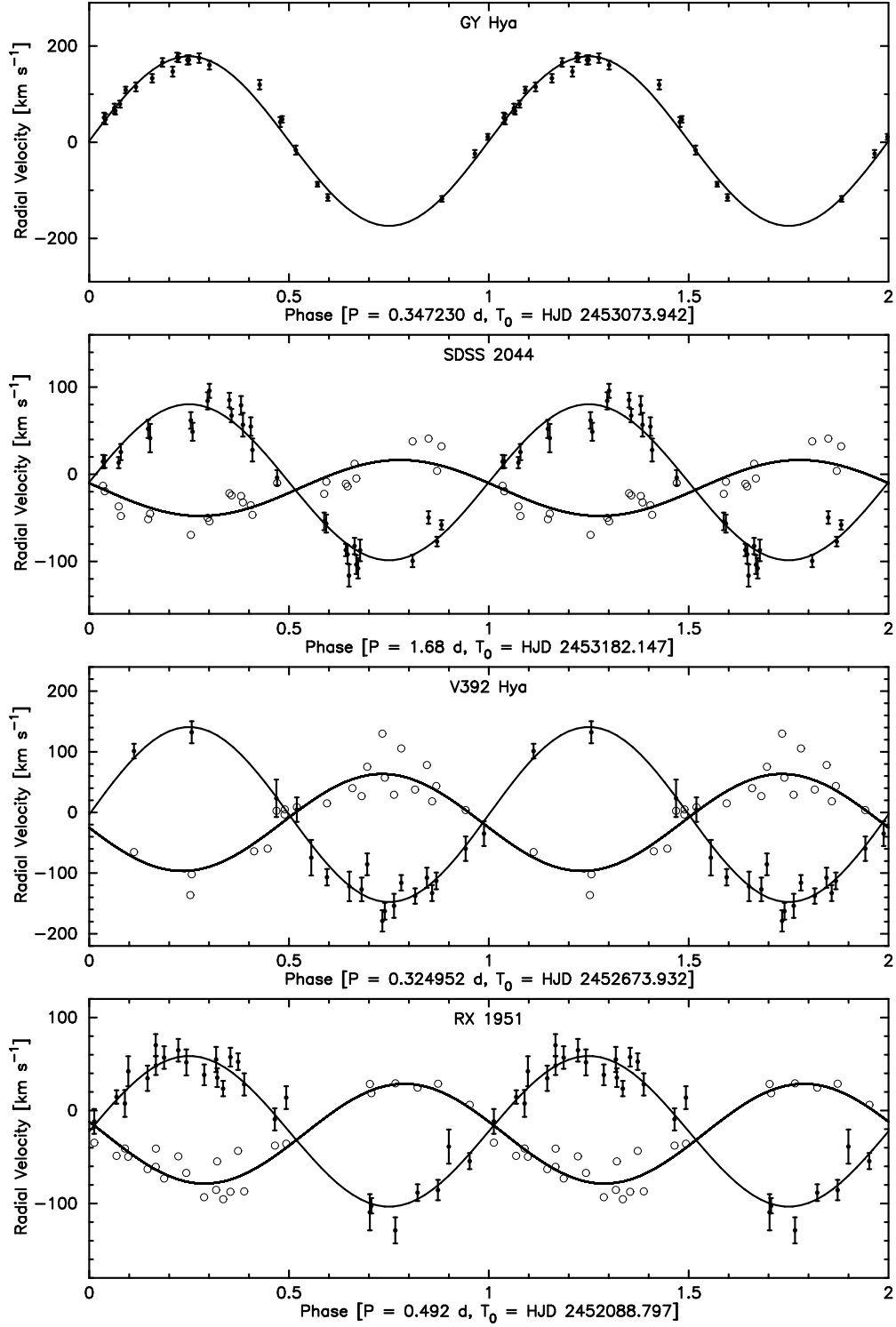
Fig. 1.— Absorption (solid dots with error bars) and emission (open circles) radial velocities folded on the adopted orbital periods. Best-fit sinusoids are superposed. All data are shown twice for continuity. For GY Hya, the curve is folded about the only available period, that of the absorption line velocities.
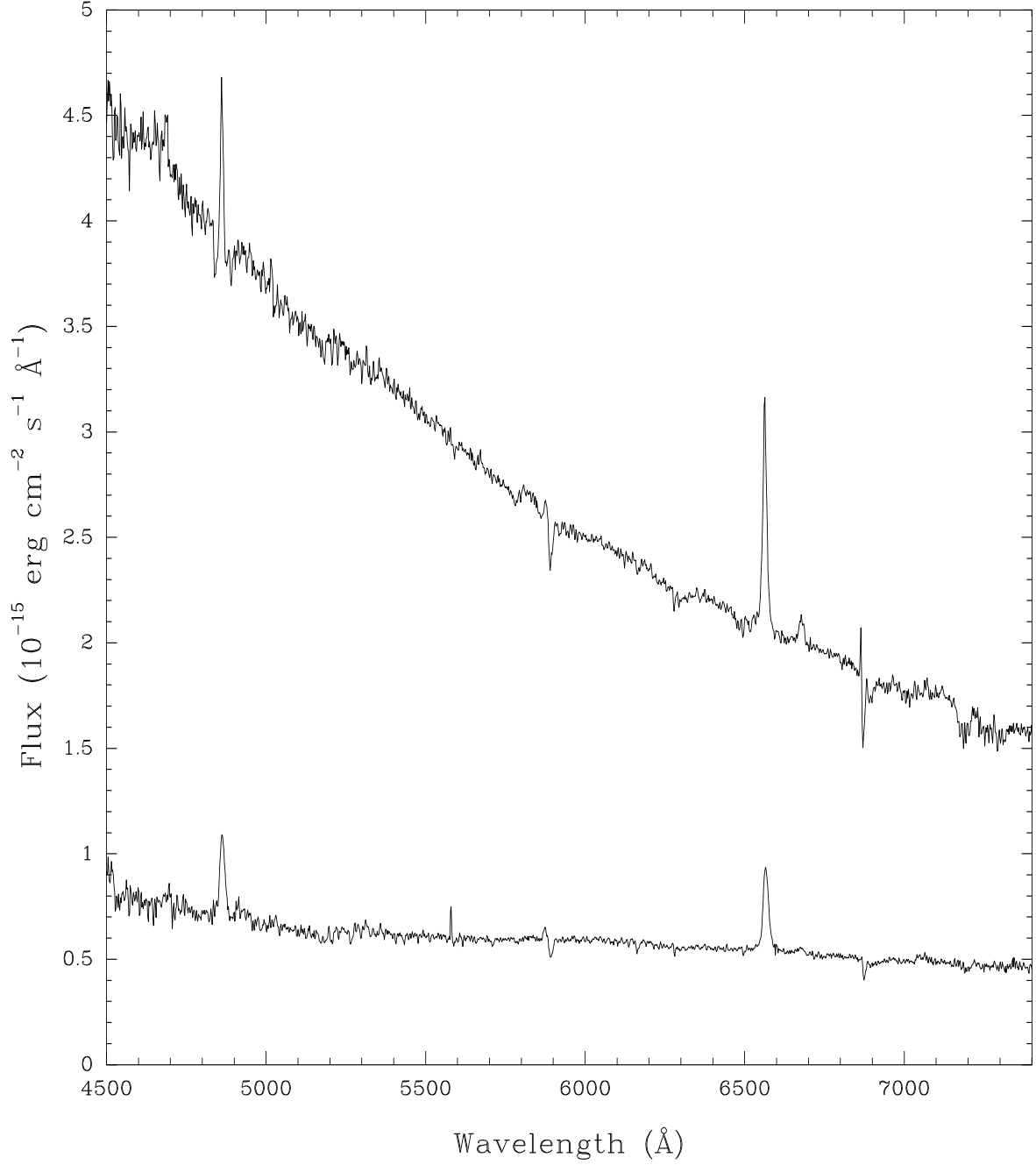
Fig. 2.— Mean spectra of V392 Hya in different states. Top/bottom spectrum was taken in 2004/2003, respectively. Note the differences in mean flux level, continuum shape, and line strength.
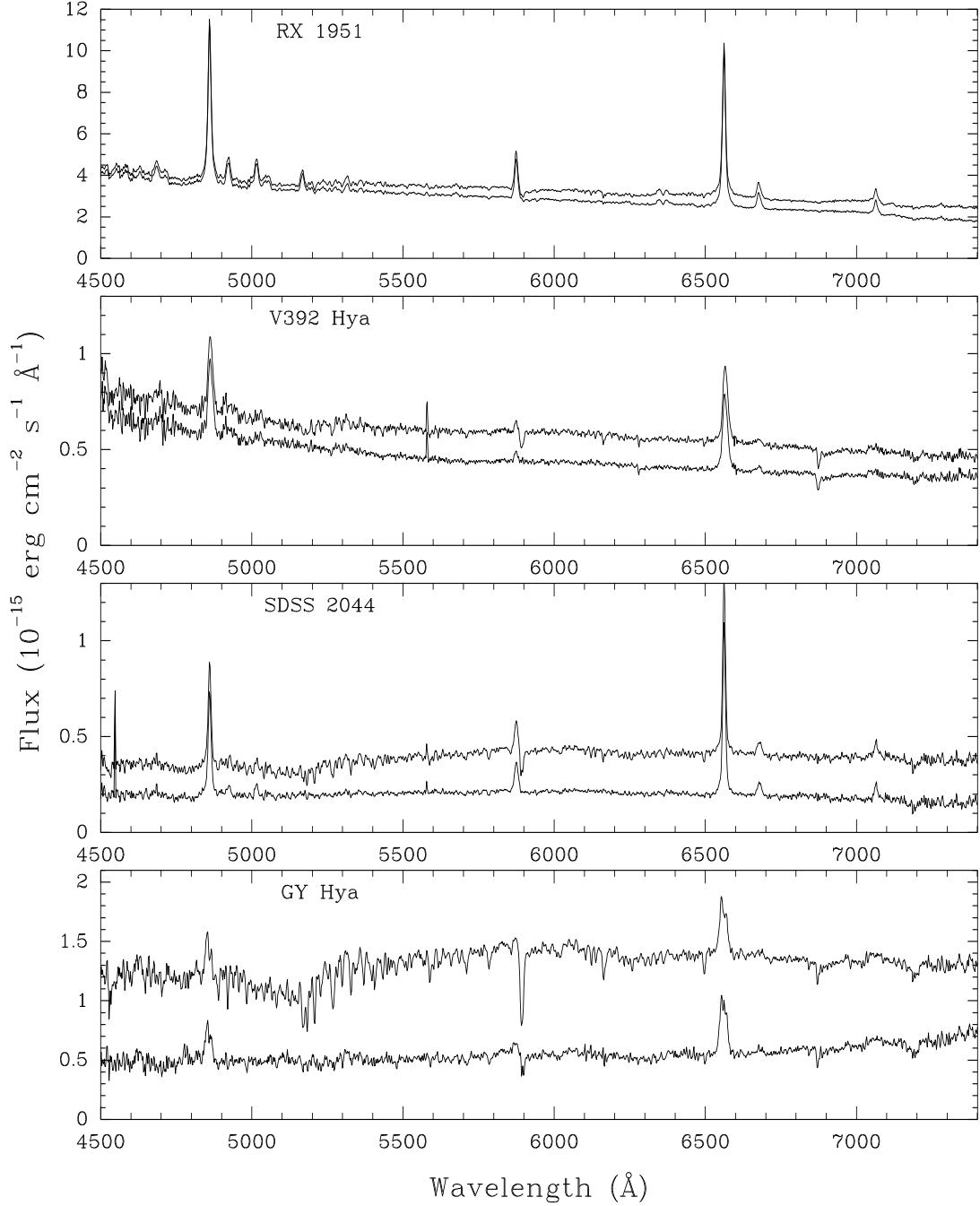
Fig. 3.— A montage of spectra. The vertical scale in each plot is in units of 10^{-15} erg s^{-1} cm^{-2} Å^{-1}, subject to calibration uncertainties of some tens of percent. The lower trace in each panel shows the data after a scaled late-type star has been subtracted away (see text and Table 5). In all cases the original spectra are shifted into the rest frame of the secondary star before averaging.